Polymer 50 (2009) 3347–3360

Contents lists available at ScienceDirect

Polymer

journal homepage: www.elsevier.com/locate/polymer

Study on morphology evolution and fractal character of the miscible blend between isotactic polypropylene and copolymer of ethylene and propylene

Xu-huang Chen [a,b], Gui-qiu Ma [a,*], Jing-qing Li [a], Shi-chun Jiang [a], Xu-bo Yuan [a], Jing Sheng [a,*]

[a] School of Materials Science and Engineering, Tianjin University, Tianjin 300072, China
[b] School of Chemical and Environmental Engineering, Hubei University of Technology, Wuhan 430068, China

ARTICLE INFO

Article history:
Received 1 December 2008
Received in revised form
27 April 2009
Accepted 29 April 2009
Available online 9 May 2009

Keywords:
iPP/mEP polymer blends
SEM pattern analysis
Fractal

ABSTRACT

The compatibility of isotactic polypropylene (iPP) with a block copolymer of ethylene and propylene (mEP) was evaluated by glass transition temperature measurements and Han curves. The morphology of the dispersed phase in alloys of iPP with mEP was observed by scanning electron microscopy (SEM). The average diameters, dp, of the dispersed phase in iPP/mEP alloys were calculated from SEM images. The results indicated that dp depends on the composition and mixing condition of the alloys. The distribution of dp was studied using graph-estimation methods and found to be log-normal in character. The calculated standard deviation, σ, characterizes the dispersed phase particle distribution width, and depends on the composition and mixing conditions of the blends. The fractal behavior of the phase morphology shown by SEM images of the alloys was studied, and the fractal dimensions were calculated by the changing coarse-graining level and measure relations methods. The self-similarity of the systems is discussed. The fractal dimensions depend on the composition and mixing conditions of the alloys.
© 2009 Elsevier Ltd. All rights reserved.

1. Introduction

Applications of many thermoplastic materials are limited by their toughness (impact resistance) [1]. The limitation can be overcome by blending the thermoplastic materials with rubbers or plastics. Many studies have been carried out on the phase structure, morphology, phase dispersion, interaction between phases (compatibility and interfacial interaction) and compatibilization of thermoplastic/rubber blends [2].

Many thermoplastic materials have been modified by elastomer [2,3], by melt mixing. In the case of polyolefin/elastomer blends, ethylene propylene rubber (EPR) or ethylene propylene diene monomer (EPDM) have been used [4–8]. Styrene–butadiene–styrene triblock copolymer (SBS) or styrene–ethylene/butylene–styrene triblock copolymer (SEBS) [9–12] elastomers have been commonly used in the modification of polypropylene (PP). These elastomers are compatible with polyolefins. The phase structure and morphology of incompatible and partially compatible blends of PP with poly(*cis*-butadiene) rubber (PcBR) and EPDM have been investigated in previous studies of our group [13–17]. Blends of a new elastomer PEOC (copolymer of ethylene and octene) have been reported recently [18–21].

The graphical technique for microscope images has been widely applied in research on the phase structure of blends [22,23]. In our group, phase structure, morphology and phase size are determined by graph processing of microscope images [14,15,24–26].

There have been many reports on the formation and evolution of phase structure and morphology during melt blending of thermoplastics with thermoplastics [27–31] However, there have been fewer reports on the formation and evolution of phase structure during melt blending of thermoplastics with elastomers. We previously studied the formation and evolution of phase structure and morphology during melt blending of polypropylene with rubber [32–34].

In the present report, the compatibility of the two components in iPP/mEPE alloys is discussed. The structure and morphology of the alloys were observed by scanning electron microscopy (SEM), and the phase size was calculated by graph processing. The fractal character of the morphology of the dispersed phase during melt blending in the iPP/mEPE alloys is discussed.

2. Experimental

2.1. Materials

Polypropylene (iPP, isotactic polypropylene 1300) was a commercial polymer (supplied by Beijing Yanshan Petrochemical Co.) with $\langle M\rangle_w = 4\times10^5$ g mol^{-1}, $\rho = 0.910$ g cm^{-3} and MI (melt

* Corresponding authors.
E-mail addresses: magq@tju.edu.cn (G.-q. Ma), ghxu@tju.edu.cn (J. Sheng).

0032-3861/$ – see front matter © 2009 Elsevier Ltd. All rights reserved.
doi:10.1016/j.polymer.2009.04.069

index) = 1.2 g per 10 min. The elastomer, a copolymer of ethylene with propylene synthesized with metallocene catalyst (mEP, VMX-1100) was a commercial material from Mobil Oil Corp. (USA), with 15% ethylene content, $\rho = 0.863\ g\ cm^{-3}$ and MI = 1.3 g per 10 min.

2.2. Preparation of blends

Binary blends of iPP and mEP were made by melt mixing the components in a mixing apparatus (XXS-30 mixer, China) at a fixed temperature with a fixed residence time and rotational speed.

The compositions of the blends were 90/10, 80/20, 70/30, 60/40, 50/50, 40/60, 30/70, 20/80 and 10/90 (iPP vol%/mEP vol%). The mixing times (minutes) used were 0.5, 0.75, 1.0, 1.5, 2.0, 3.0, 4.0, 6.0, 8.0 and 10.0 at 200 °C and shear rate $51.2\ s^{-1}$. For the iPP(80)/mEP(20) alloy, mixing temperatures 180, 190, 200, 210 and 220 °C were used at shear rate $51.2\ s^{-1}$, and shear rates (s^{-1}) 25.6, 51.2, 76.8, 102.4 and 128 were used at 200 °C mixing temperature.

2.3. Specimen preparation

The pre-blended samples were rapidly immersed in liquid nitrogen, removed after 30 min and fractured, then the fracture surfaces were etched with cyclohexane prior to examination by SEM. The premixed material was compression molded at 190 °C and 20 MPa for 1 min to get films of 0.5 mm thickness and diameter 20 mm for rheological analysis.

2.4. Characterization

A scanning electron microscope (SEM, Philips XL30) operated at 20 kV accelerating voltage was used to examine the fracture morphology of the blends. The fracture surface of samples was coated with gold for microscopic observation, to ensure that the etched surface structure of the blends was intact.

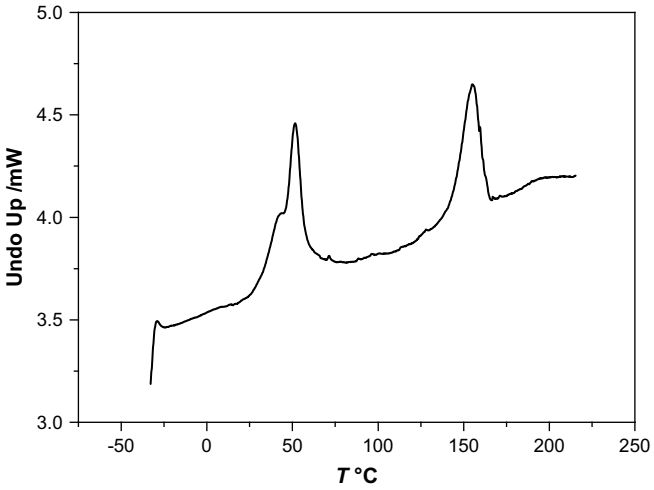

Fig. 2. DSC curve of metallocene–ethylene propylene elastomer.

The glass transition temperature, T_g, of the blends was obtained by dynamic thermomechanometry using a Q800 TA DMA (dynamic mechanical analyzer), TA Instruments, USA.

A Rheological Instruments AB, Sweden, instrument was used to determine rheological properties.

2.5. Data collection

Particle size data were obtained from SEM images using digital process software (EMPP) edited by our group. The software treats only binarized images: black particles for instance, are distributed in a white matrix. Such images can be difficult to obtain because accurate binarization requires a clear initial image with good

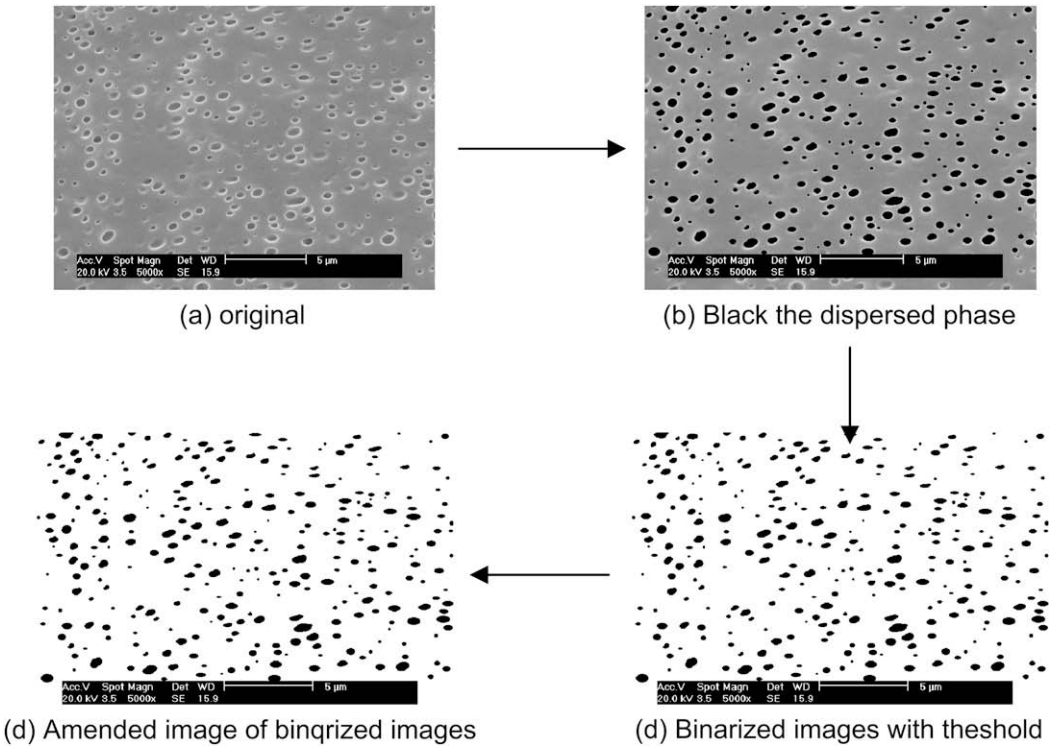

Fig. 1. SEM and corresponding binarized image of PP/mEP (80/20) blends.

Table 1
T_g of PP/mEP blends.

Content of PP/%	100	90	80	70	60	50	40	30	0
T_g1/°C				−9.53	−11.74	−12.05	−12.18	−12.37	−15.56
T_g2/°C	16.46	15.76	12.35	11.28	10.56				

contrast between matrix and particles. Here we focus on the data treatment once the image has been binarized. A detailed binarizing process used in this study is shown in Fig. 1.

The cross-sectional area of particles was determined using image analysis software for SEM images. An equivalent diameter,

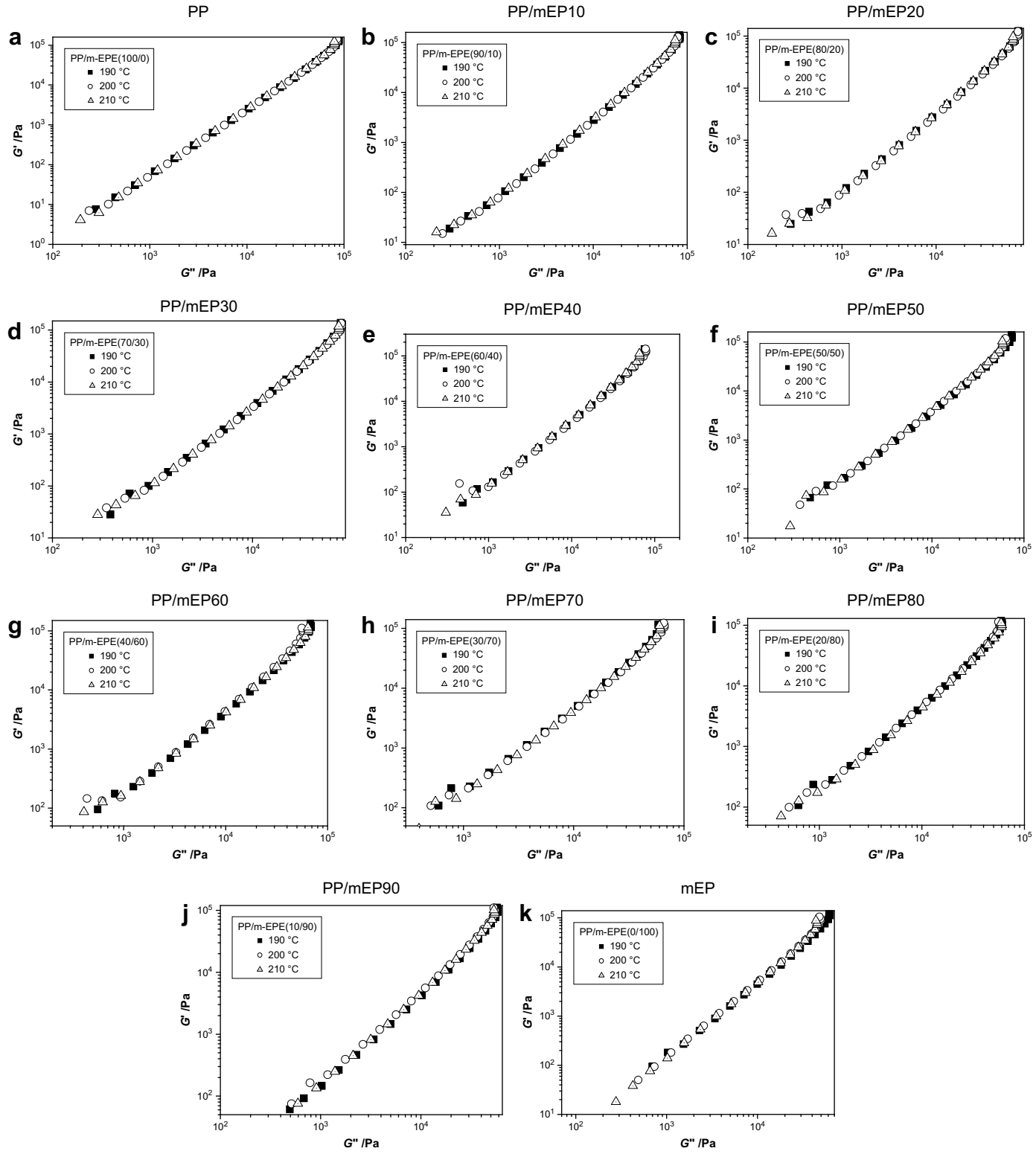

Fig. 3. The relation between G' and G'' with compositions at different temperature.

dp, was defined for each particle as the diameter of a circle with the same cross-sectional area [35]:

$$S = \sum_{i=1}^{M} S_i \tag{1}$$

$$\mathrm{dp} = \sqrt{\frac{4s}{\pi}} \tag{2}$$

3. Results and discussion

3.1. Compatibility of the blends

Fig. 2 shows a differential scanning calorimetry (DSC) scan of mEP during melting, showing a peak at 52 °C that is identified with the melting transition of the polyethylene chain segments (blocks) in mEP. The peak at 155 °C is the melting transition of the polypropylene blocks. It was expected that the alloys would show compatibility between mEP and iPP.

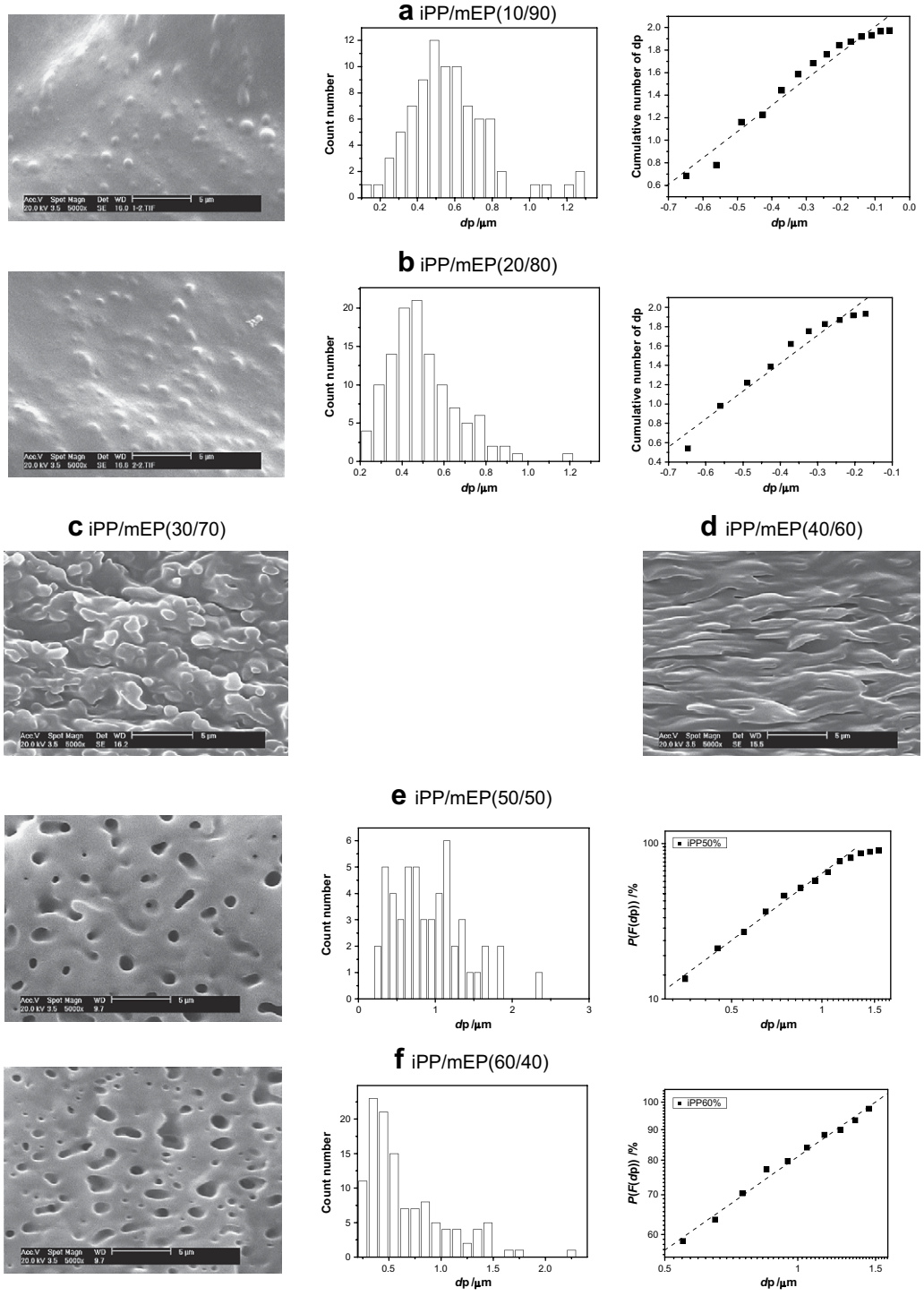

Fig. 4. SEM image and distribution image of dp on PP/mEP blends.

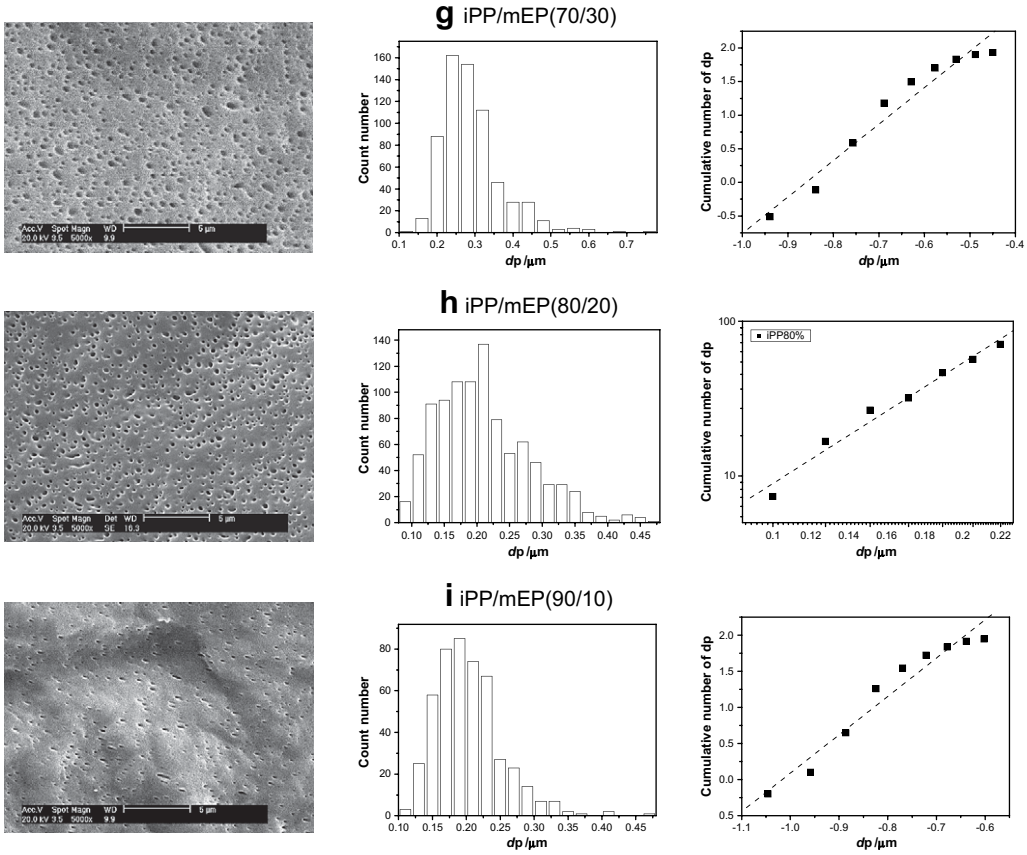

Fig. 4. (*continued*).

The glass transition temperature, T_g, was measured by DMA at 3 °C min^{-1} scan rate. These results are shown in Table 1, and indicate that the glass transition temperature of iPP, T_{giPP}, was 16.46 °C, and T_{giPP} decreased with increasing mEP content in the alloys. The glass transition temperature, T_{gmEP}, of mEP was −15.56 °C, and T_{gmEP} increased with increasing iPP content. It is clear that iPP and mEP are partially miscible.

Han curves, i.e. plots of the relaxation modulus, G', versus loss modulus, G'', for different temperatures, were obtained from rheological data for iPP/mEP alloys; the data are shown in Fig. 3. The Han curves [35–37] characterize the compatibility of the system in polymer blends. If the microstructure does not depend on the temperature of the system, so that the relationship between G' and G'' is the same at different temperatures, the system should be compatible or partially compatible. Fig. 3 reveals these results, showing Han curves that are coincident and implying that mEP is partially compatible with iPP.

3.2. SEM studies

3.2.1. Formation of the phase morphology during melt blending

Etching of microscopically fractured surfaces of the alloys with cyclohexane removed the elastomer component, leaving black holes. Fig. 4 shows SEM images of iPP/mEP alloys with varying composition. In alloys with iPP content <20%, iPP was the dispersed phase corresponding to the spherical or ellipsoidal protuberances distributed uniformly throughout the sample. The elastomer (mEP) was the dispersed phase when the iPP content was >50%, corresponding to the uniformly distributed cavities. The phase-inversion region is from 30/70(iPP/mEP) to 40/60(iPP/mEP), showing the structure and morphology of double continuous phases in that range of compositions.

The average diameter, dp, of the dispersed phase was calculated by graphical processing and equation (2) as shown in Fig. 5. There are three regions in Fig. 5. In region A, iPP is the dispersed phase and dp increases with increasing iPP content. In region B, mEP is the dispersed phase and dp decreases with increasing iPP content. Region C corresponds to the double continuous phase.

Fig. 6 shows the time evolution of SEM images of iPP(80)/mEP(20) alloys. The calculated values of dp, shown in Fig. 7,

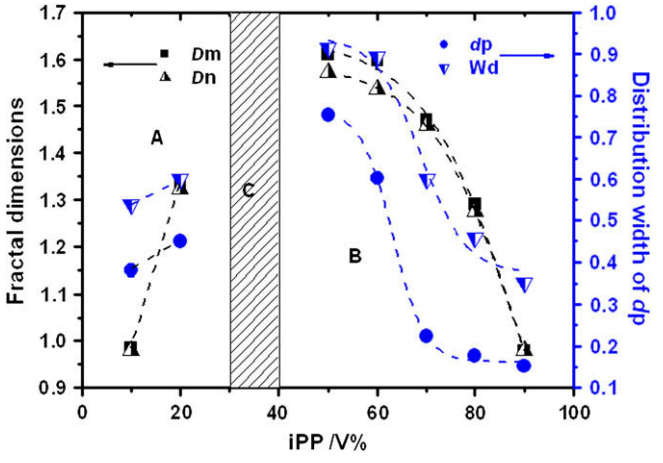

Fig. 5. The relation of average diameter dp and distribution width of dp in iPP/mEPE.

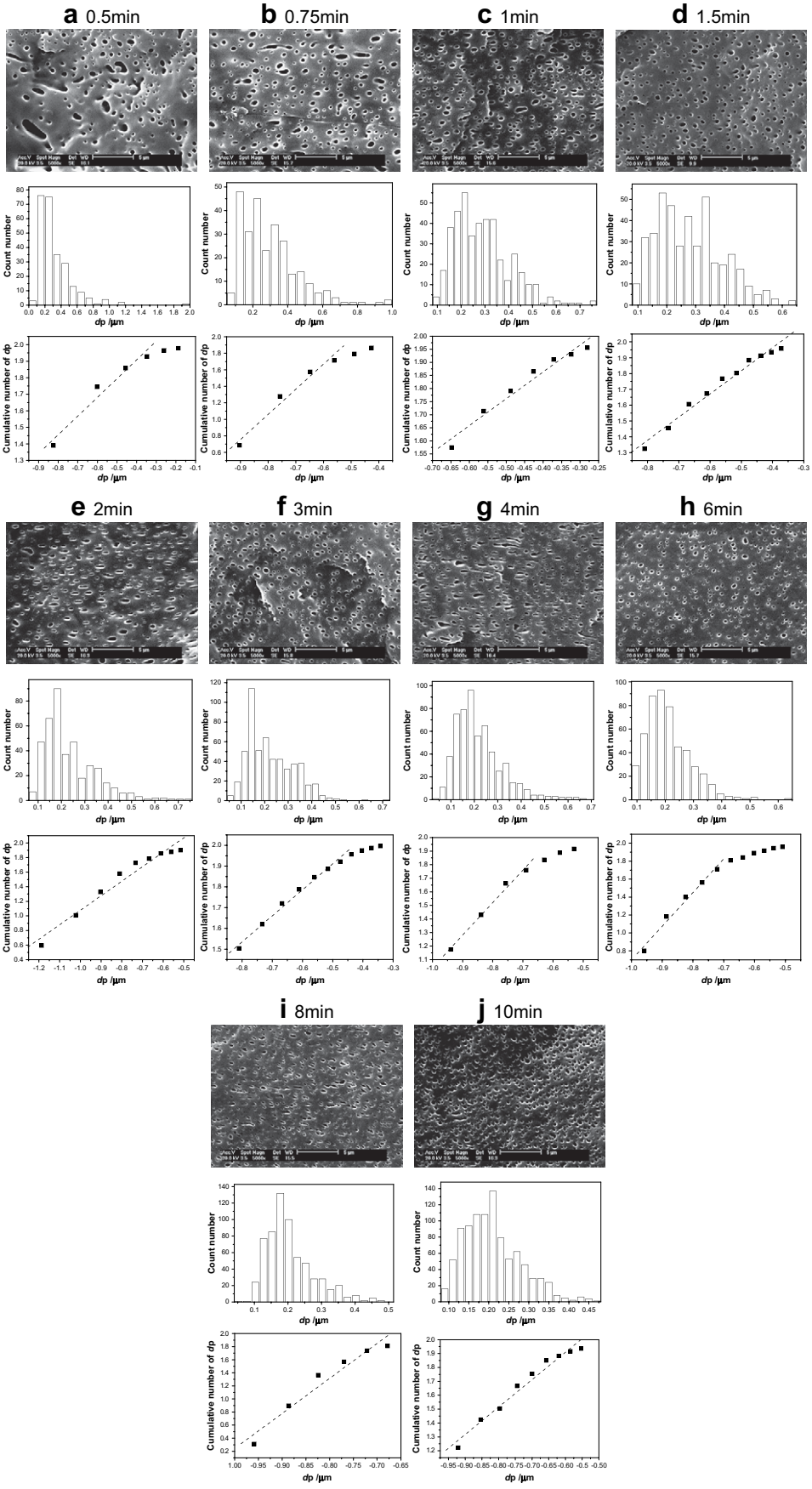

Fig. 6. SEM image and distribution of dp for mixing time in iPP/mEP blends.

decrease with increasing mixing time. The three regions in Fig. 7 are interpreted as follows: in region I, the initial mixing stage, dp of the dispersed phase decreases rapidly, showing that the particles of the dispersed phase are broken up and converted to small particles. In region II, the mid-term mixing stage or transition stage, the size of the dispersed phase particles decreases slowly with increasing mixing time. In this mixing stage there is increased probability of collision between particles as the number of dispersed phase particles increases. The rate of increase in the number of particles, hence reduction in average particle size, is partially offset by collision induced coalescence of particles. In region III, the late mixing stage, the fluctuations of dp vary only slightly with increasing mixing time because of the dynamic equilibrium between particle breakup and coalescence.

SEM images for iPP(80)/mEP(20) alloys formed at a range of mixing temperatures are shown in Fig. 8. The variation of dp with mixing temperature has a minimum at 200 °C.

Fig. 10 shows SEM images for iPP(80)/mEP(20) alloys melt blended at a range of shear rates. The variation of dp with shear rate, shown in Fig. 11, indicates a minimum in dp at 51.2 s^{-1} shear rate.

3.2.2. Distribution of average particle size

An equivalent diameter, dp, of the dispersed phase in the alloys was obtained from binarized images. The probability density, $P(\mathrm{dp})$, for each dp of the dispersed phase in the blends can be defined by:

$$P(\mathrm{dp}) = \frac{N(\mathrm{dp})}{\int_0^\infty N(\mathrm{dp})\mathrm{d}(\mathrm{dp})} \tag{3}$$

where $N(\mathrm{dp})$ is the frequency of occurrence of diameter dp. Histograms of $P(\mathrm{dp})$ versus dp characterize the distribution of dp. For many particle dispersions [38] and particles of phases in polymer blends in particular [39], the distribution of particle sizes obeys a log-normal distribution. The distribution of particle size can be ascertained from statistical laws, as in graph-estimation methods. According to graph-estimation theory (see Appendix A), a log-normal distribution function corresponds to an ascending line in the X–Y coordinate system. Thus one can use the one to one relationship to determine whether the distribution of dp is log-normal.

$P(\mathrm{dp})$–dp histograms and a plot of $F[P(\mathrm{dp})]\%$ versus dp for iPP/mEP alloys are shown in Fig. 4. The ascending lines show that the distribution of dp is log-normal. Based on equation. (A4), σ for the distribution function of dp can be obtained by linear regression. σ characterizes the distribution width of dp (see Appendix A). Fig. 5 shows that σ depends on the composition of the alloys. The variation of σ is similar to that of dp (increase with increasing content of dispersed phase) but the variation range of σ is smaller compared with dp.

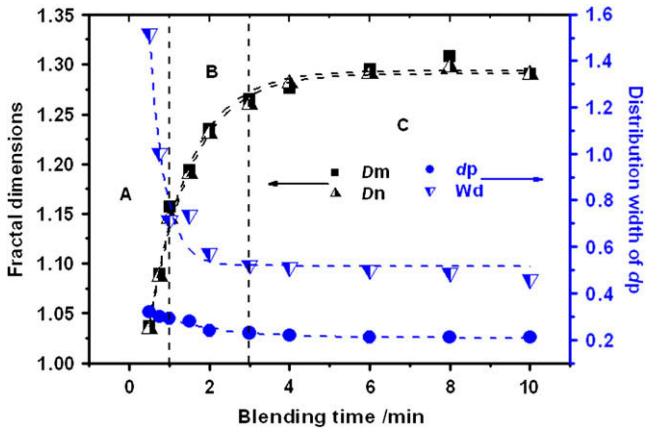

Fig. 7. The variation of average diameter dp and distribution width of dp with mixing time during melt mixing for iPP80/mEP20 blends.

Fig. 6 shows the distribution of dp, as $P(\mathrm{dp})$–dp histograms and a plot of $F[P(\mathrm{dp})]\%$ versus dp, as a function of mixing time for iPP(80)/mEP(20) alloys. The ascending lines show that the distribution of dp with mixing time is a log-normal distribution. σ, shown in Fig. 7, decreases rapidly with increasing mixing time in region I. In the mid-term mixing stage σ at first increases with increasing mixing time, and fluctuates thereafter. SEM images (Fig. 6) show that the morphology of the dispersed phase varies but the variation in particle size for the dispersed phase is small. In the late mixing stage σ decreases slowly with increasing mixing time.

For different mixing temperatures and shear rates, the distributions of dp are also log-normal distributions, for iPP(80)/mEP(20) blends (see Figs. 9 and 11). The width of the distribution of dp varies with mixing temperature and shear rate, and shows minima at a particular temperature and shear rate.

3.3. Fractal behavior

In multi-component polymer blends, due to the nonlinear character of the phase morphology the phase distribution of the blends is discussed in terms of nonlinear mathematics via a fractal dimension introduced by Takayasu [40]. For this purpose, the SEM micrographs were binarized and particles of the dispersed phase abstracted. The fractal dimension was calculated from binarized SEM patterns, applied changing coarse-graining level (called box-counting) and measure relations methods (see Appendices B and C).

As in the changing coarse-graining level method, we cover points distributed in space with squares (tiles) whose border length is r, and count the number of squares that contain at least one point. This number is denoted by $N(r)$. If $N(r)$ satisfies the relation

$$N(r) \propto r^{-D} \tag{4}$$

the results are independent of the form of the tiles. A plot of $\log N(r)$ versus $\log r$ should lead to a straight line with slope Dn (see Fig. 12), i.e. the fractal dimension. In addition, the fractal dimension Dm was calculated by measure relation methods. The variation of Dn and Dm with composition shown in Fig. 5 indicates that Dn and Dm are similar. The variation of Dn and Dm with the composition of the alloys is similar to that of dp.

The fractal dimensions, Dn and Dm, obtained by changing coarse-graining level and measure relation methods characterize the particle distribution density of the system. In iPP/mEPE alloys dp and σ increase with increasing dispersed phase content, i.e. the number of dispersed phase particles is increased, the particle density distribution is increased and Dn and Dm are increased.

When the morphology of an alloy possesses fractal character, the distribution of dp should have a dimensionless region, the self-similar region, in which some characteristic, e.g. the normalized shape, of the fractal object does not change with variation of scale [40–42]. As stated earlier, the scaling functions, $S(r)$, can be used to study the self-similarity. Fig. 13 shows the changing trend of two different scaling functions. As r increases, $S_M(r)/S_M(r)_{\max}$ and $S_N(r)/S_N(r)_{\max}$ both fluctuate within a small range for different compositions of the alloys, which indicates that the phase morphology has self-similarity in the dimensionless region.

Fig. 14 shows a plot of $\log N(r)$ versus $\log r$: the fractal dimensions, Dn and Dm, were calculated as shown in Fig. 7. The variation

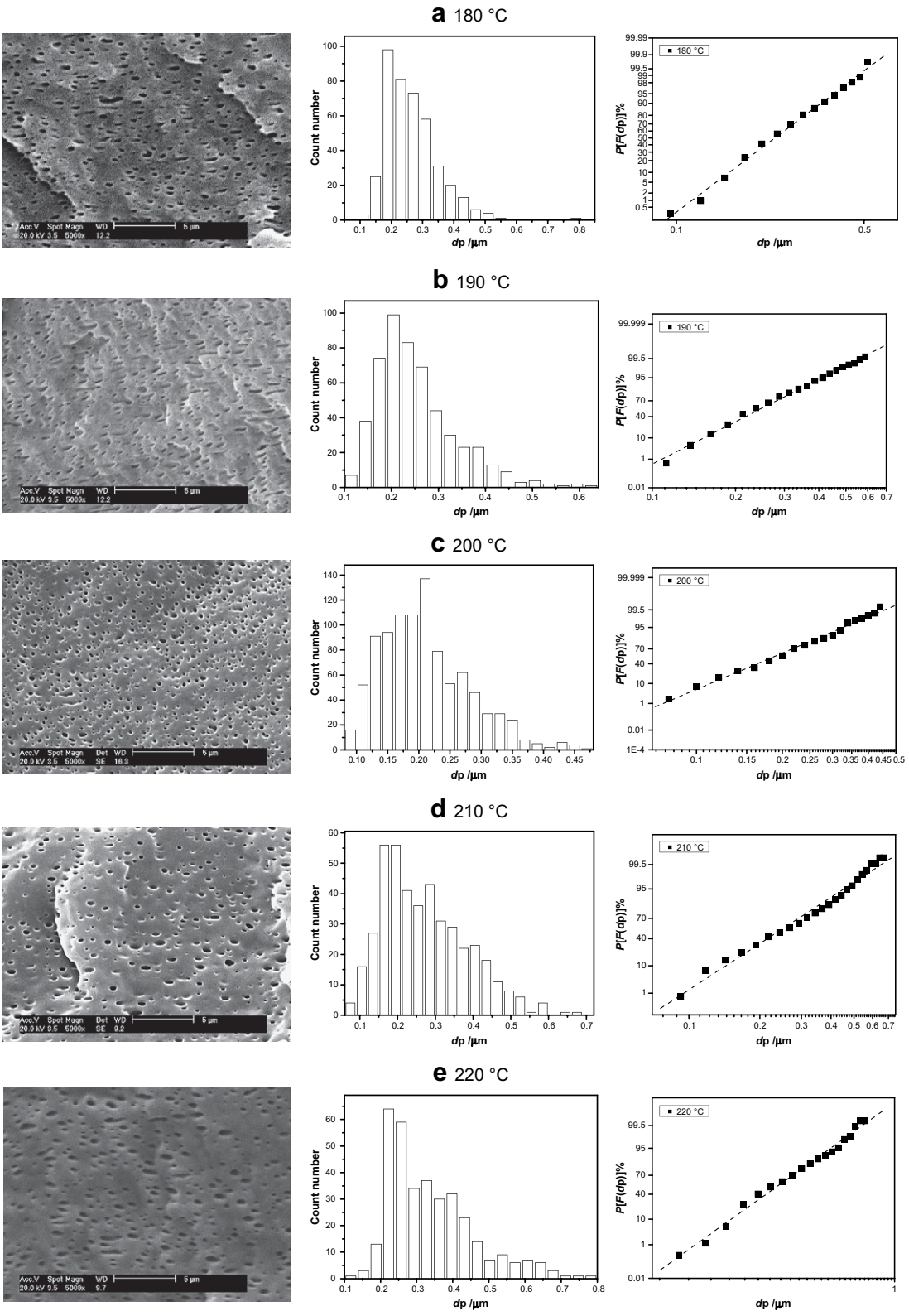

Fig. 8. SEM images and distribution of dp for mixing temperature in PP/mEP blends.

of Dn and Dm with mixing time is the same as that of dp. In the early mixing region I, Dn and Dm increase rapidly with increasing mixing time, so the density of the dispersed phase increases rapidly for iPP(80)/mEP(20). In region II, the rate of dispersed phase particle size reduction decreases, because the rate of coalescence between particles is increased. However, the rate of dispersion is still greater than the rate of coalescence. In region III, Dn and Dm show maxima with increasing mixing time due to the dynamic

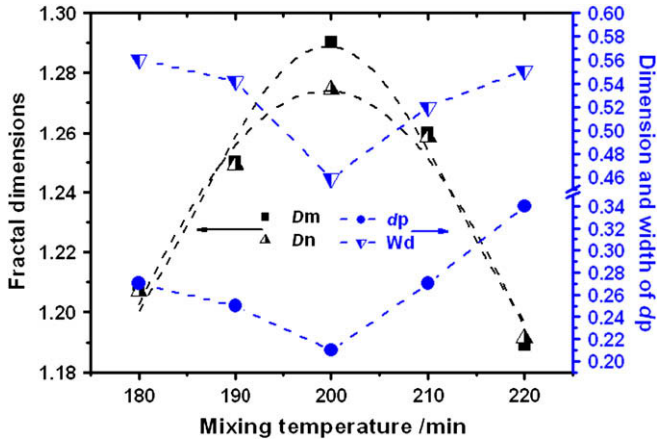

Fig. 9. The relation of the variation of average diameter dp and distribution width of dp with mixing temperature during melt mixing for iPP80/mEP20 blends.

equilibrium between particle breakup and coalescence, whereas dp has a minimum value.

In addition, the variation of phase morphology with mixing temperature and shear rate of the mixer show self-similarity (see Figs. 15–17). The variation of Dn and Dm with mixing temperature and shear rate shows maxima corresponding to minima in dp and σ (see Figs. 9 and 11), where the degree of dispersion of the dispersed phase and the distribution of dp are uniform in the alloys.

In statistical mechanics entropy is a measure of the degree of disorder or confusion and randomness in a system. Entropy increases with increasing degree of disorder in the multi-component system. For example, the formation and evolution of the phases in the alloys during melt blending show that the dispersed phase is changed into small particles and the number of dispersed phase particles is increased, so the particle density and degree of disorder, hence entropy of the system are increased. The fractal dimension shows the density of systems from above. The fractal dimension, Dn or Dm, is another measure of the entropy, and Dn and Dm have the physical meaning of entropy.

4. Conclusions

Because mEP is a block copolymer of ethylene with propylene it was expected that mEP and polypropylene should show compatibility. In accordance with that expectation, the glass transition temperature data and Han curves show partial miscibility in alloys of mEP with isotactic polypropylene.

SEM images of the surfaces of cryoscopically fractured samples show that the average diameter, dp, of the dispersed phase of the alloys, obtained by graphical processing, varies with mixing conditions during melt blending. The average diameter, dp, of the dispersed phase has a log-normal distribution.

The variation of morphology in iPP/mEP alloys during melt blending has been studied via the structure function, which shows self-similarity. Consequently, the variation of morphology possesses fractal character in a dimensionless region, and the fractal dimension could be evaluated in conjunction with the variation of the structure and morphology during melt blending. The fractal dimensions, Dn and Dm, were calculated by box-counting and measure relations methods that show the particle density of the alloy system, and provide a measurement of entropy, which is a state function determined by the degree of confusion of the phase structure. Finally, the quantitative description of the morphology during formation and evolution of phase structure in the alloys is related to the randomness due to fractal dimensions. Dm and Dn have the meaning of entropy.

Acknowledgment

The authors gratefully thank the Natural Science Foundation of China (contract grant number 50390090) and the Science and Technology Committee of Tianjin, China (contract grant number 05YFJMJC09100) for their support.

Appendix A. Figure-estimation theory of log-normal distribution

The graph-estimation methods [43] introduced to study the distribution of dp allow a judgment to be made as to whether the distribution of a variable is a log-normal distribution.

If t is a positive random variable and $\ln t \sim N(\mu,\sigma^2)$ then t obeys a log-normal distribution, represented by $t \sim \ln(\mu,\sigma^2)$. Here μ is the expectation value and σ^2 is the variance. The magnitude of σ reflects the distribution range of t: the larger is σ, the broader the distribution. Ordinarily, the logarithm in a log-normal distribution is the natural logarithm, and the distribution function of the log-normal distribution is given by:

$$F(t) = \frac{\log e}{\sqrt{2\pi}\sigma t}\int_{-\infty}^{t} \exp\left[-\frac{1}{2}\left(\frac{\log t-\mu}{\sigma}\right)^2\right]\mathrm{d}t, t>0 \tag{A1}$$

This function is monotonic ascending in the $t-F(t)$ coordinate system. It can be described by the standard normal distribution function as follows:

$$F(t) = \int_{-\infty}^{\frac{\log t-\mu}{\sigma}} \frac{1}{\sqrt{2\pi}} e^{-\frac{x^2}{2}}\mathrm{d}x = \Phi\left(\frac{\log t-\mu}{\sigma}\right), t>0 \tag{A2}$$

$$\Phi^{-1}[F(t)] = \frac{\log t-\mu}{\sigma} \tag{A3}$$

If we denote $\Phi^{-1}[F(t)]$ by Y and $\log t$ by X, then formula (A3) can be changed to:

$$Y = \frac{1}{\sigma}X - \frac{\mu}{\sigma} \tag{A4}$$

where X and Y are the parameters in the X–Y coordinate system. Equation (A4) corresponds to a straight line in the X–Y reference frame whose slope and intercept are $1/\sigma$ and $-\mu/\sigma$, respectively. σ is the standard deviation, and characterizes the width of the dispersed particle size distribution, and μ is number average of the distribution in $\log t$. Thus, the relationship between a log-normal distribution function and an ascending straight line in the X–Y reference frame is found, which is described as the graph-estimation method. Based on the method, it can be judged whether the distribution of sizes of the dispersed phase particles is a log-normal distribution, and the width of the size distribution can be obtained.

Appendix B. Fractal theory by changing coarse-graining level [40]

Many physically feasible methods of defining dimension have been devised recently, and changing coarse-graining level (box-counting) is one such method.

We cover points distributed in space with squares whose border length is r and count the number of squares, $N(r)$ that contain at least one point. If $N(r)$ satisfies the relation

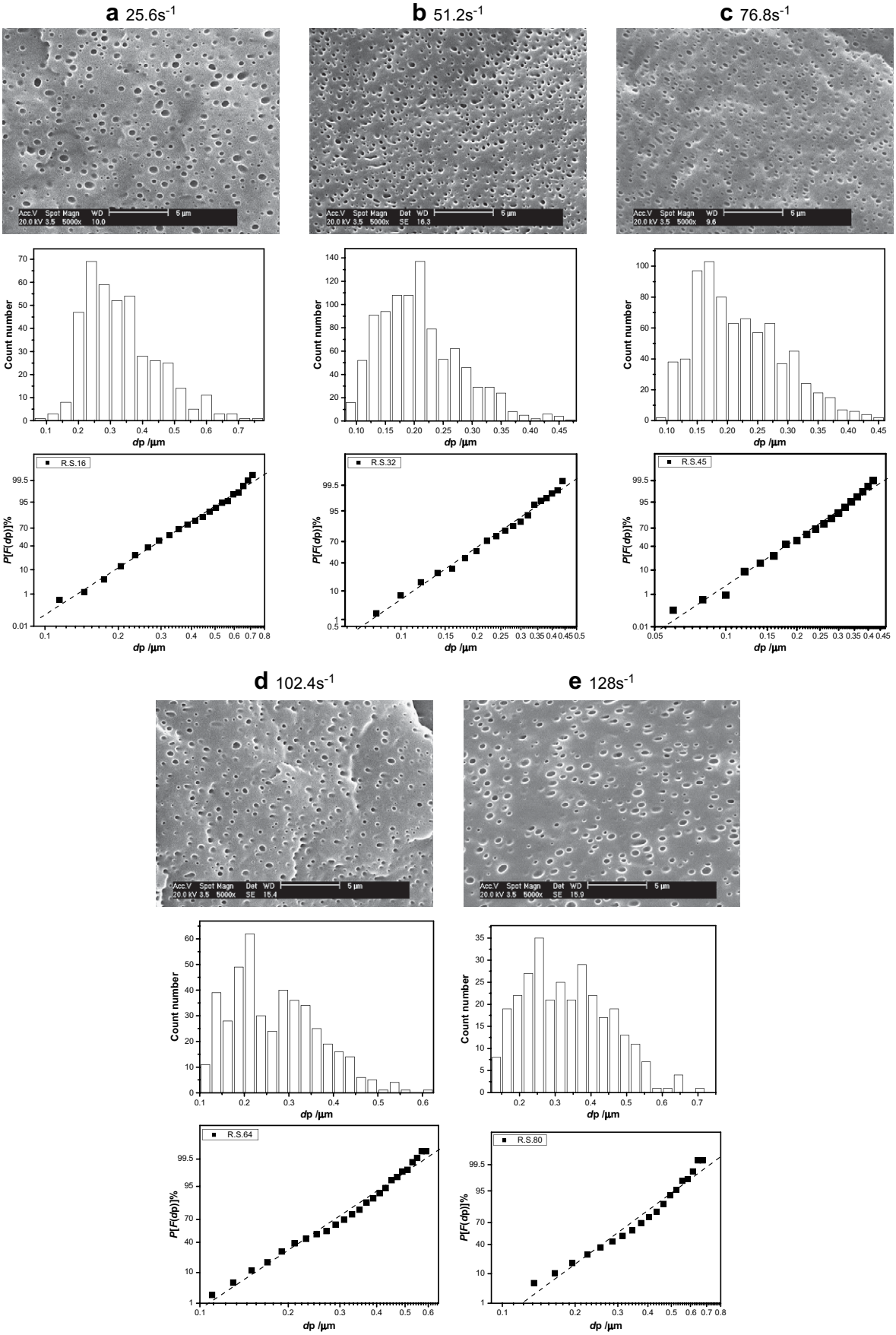

Fig. 10. SEM images and distribution of dp for rotational speeds in PP/mEP blends.

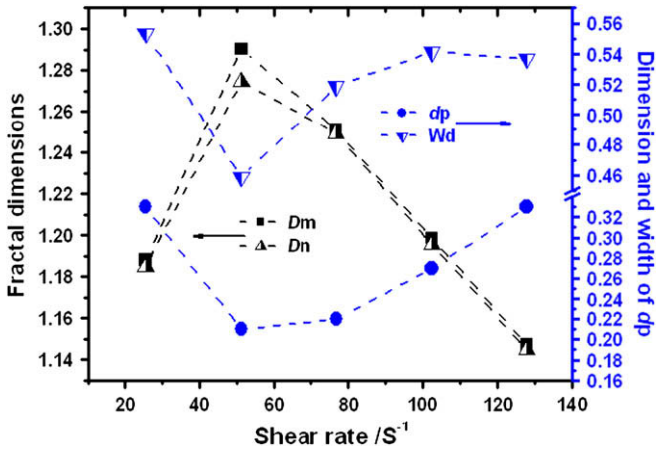

Fig. 11. The relation of average diameter dp and distribution width of dp with shear rate during melt mixing for iPP80/mEP20 blends.

$$N(r) \propto r^{-D} \tag{B1}$$

when r changes, we say this distribution of points is D-dimensional, and we call D the fractal dimension. To study the fractal behavior of the phase morphology, we cover the SEM micrograph with such squares

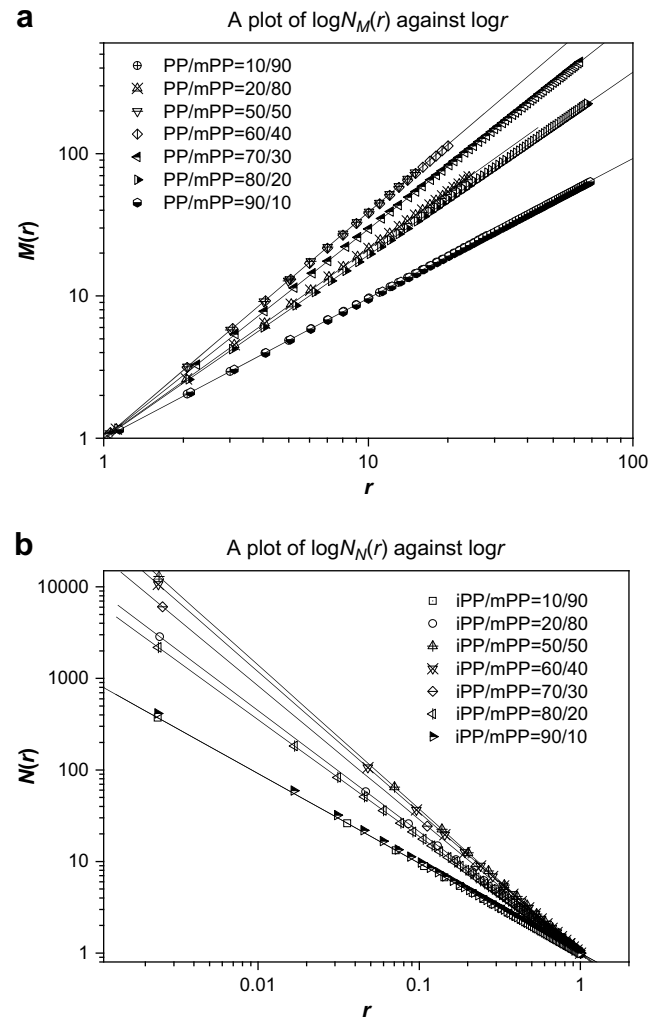

Fig. 12. A plot of log $M(r)$ and log $N(r)$ against log r and the fractal dimensions D of the phase morphology in iPP/mEP blends.

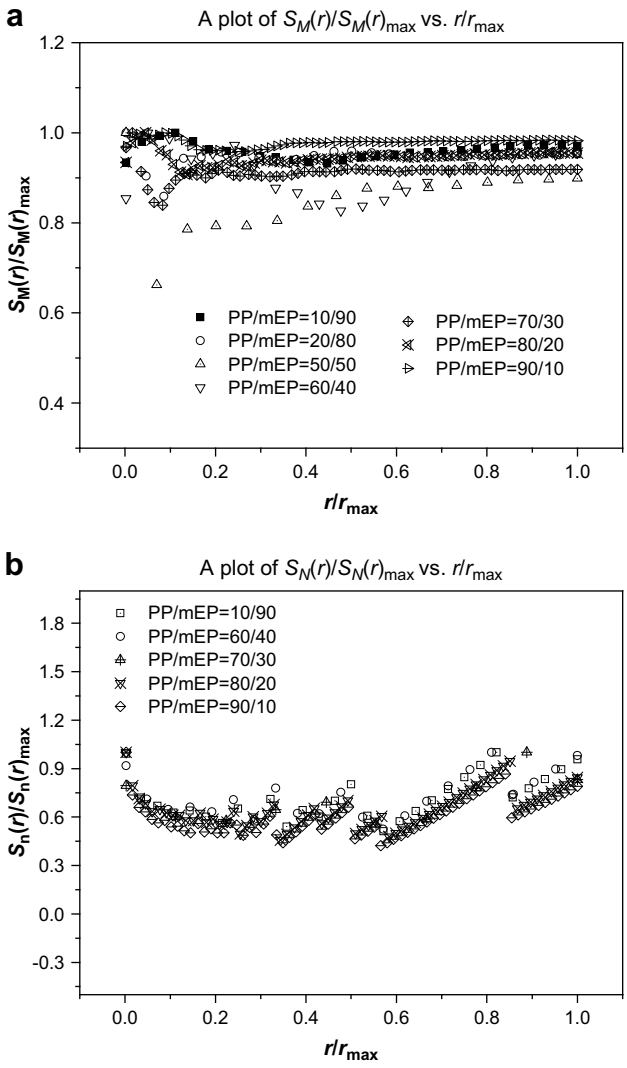

Fig. 13. Scale function $S_M(r)/S_M(r)_{max}$ and $S_N(r)/S_N(r)_{max}$ with composition in the blends.

and evaluate the corresponding $N(r)$ and r. Based on the box-counting method, the fractal dimension can be obtained. A plot of log $N(r)$ against log r should lead to a straight line with slope D. When the dispersed phase completely fills the pattern D is 2, otherwise D is between 1 and 2. D becomes larger with increasing particle distribution density of the dispersed phase. For a certain composition fraction, the greater the degree of dispersion of the dispersed phase the larger is D.

Equation (B1) describes a curve which is similar to the Koch curve [40]. Thus, in general, if a certain curve fits equation (B1), the fractal dimension D can be deduced.

To confirm self-similarity of the phase morphology, the scale function $S_N(r)$ is defined by Formula (B2) [44].

$$S_N(r) = N(r) \cdot r^D \tag{B2}$$

If $S_N(r)$ fluctuates within a small range when r changes, it means that $N(r)$ is proportional to r^{-D} (the phase morphology has self-similarity). Thus, the fractal dimension can be obtained by plotting log $N(r)$ against log r.

Appendix C. Measure relations methods [40]

For the distribution of a set of points in space, for instance the distribution of stars in the universe, we can define the fractal

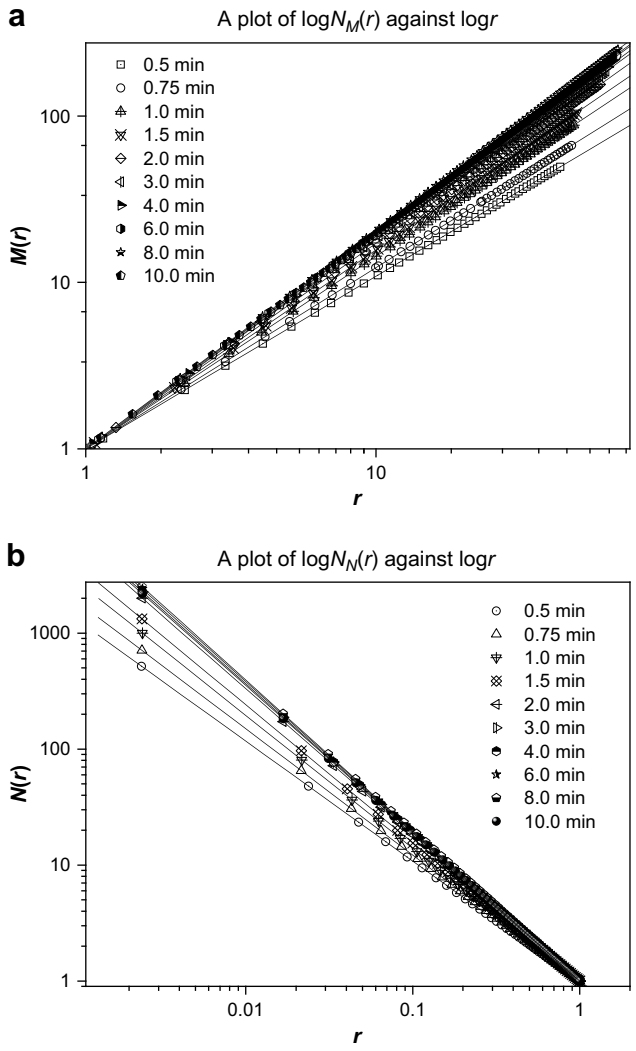

Fig. 14. A plot of log $M(r)$ and log $N(r)$ against log r and the fractal dimensions D of the phase morphology in PP80/mEP20 blends with mixing time.

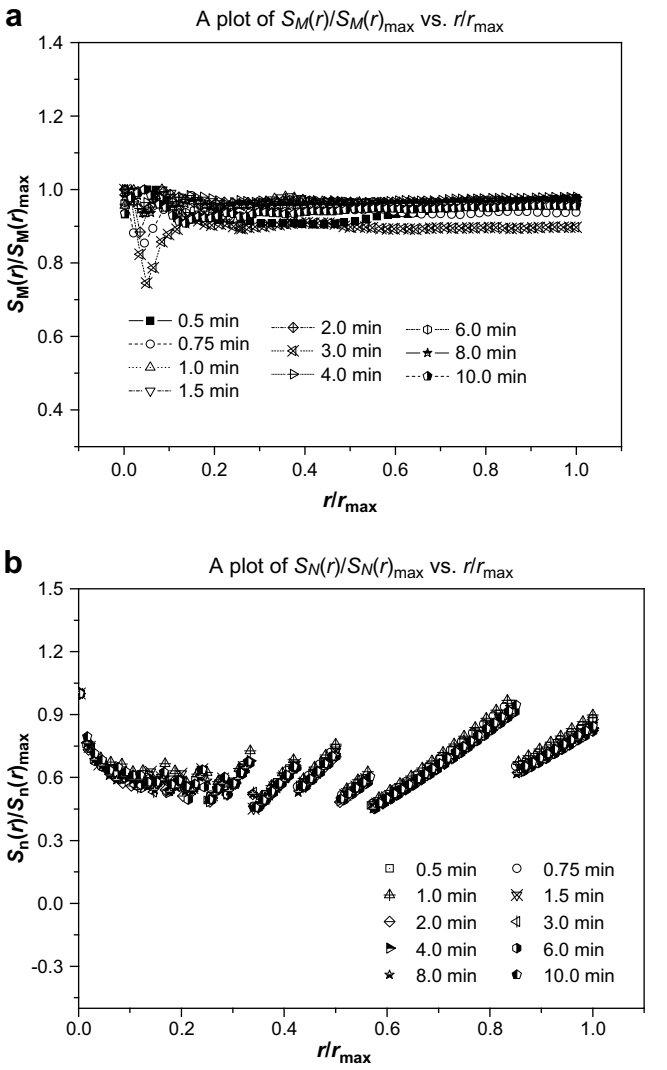

Fig. 15. Scale function $S_M(r)/S_M(r)_{max}$ and $S_N(r)/S_N(r)_{max}$ with mixing time during melt mixing.

dimension in a similar manner. Consider a sphere of radius r. We denote the number of points which is included in the sphere by $M(r)$. If the points fall on a straight line and are distributed uniformly, $M(r)$ will be proportional to r; $M(r) \propto r^{-1}$. If the distribution of points is plane-like, then $M(r) \propto r^2$. For points distributed uniformly over three-dimensional space, $M(r)$ should be proportional to r^3. By generalizing these relations, we may say the fractal dimension of the distribution of points is D if the equation

$$M(r) \propto r^D \tag{C1}$$

is satisfied. Formula (C1) can be changed to

$$D = \frac{\log M(r)}{\log r} \tag{C2}$$

and the fractal dimension can be obtained by plotting $\log M(r)$ against $\log r$.

To distinguish two different phases on SEM micrographs, the micrographs of samples for different times and shear rates were binarized. The particles of the dispersed phase can be regarded as a set of points distributed on a plane according to this theory. We can draw a square, noting the length of the square's border, r, and the number of the dispersed particles included in the square, $M(r)$. For a certain r, by changing the position of the square on the SEM micrograph we generate a set of numbers $M(r)_1, M(r)_2, M(r)_3 \ldots M(r)_n$ of the dispersed particles. To obtain better statistics, we define the number of the dispersed particles included in the square of a certain border length by Formula (C3).

$$M(r) = \sqrt[n]{M(r)_1 M(r)_2 M(r)_3 \cdots M(r)_n} \tag{C3}$$

By changing the length of the square's border, we may obtain a set of different $M(r_1)$, and the fractal dimension, D, can be obtained by plotting $\log M(r)$ against $\log r$.

When we actually try to find the fractal dimension for a set of dispersed particles, a problem occurs as to how to measure the length of the square's border. In fact, since these particles are regarded as units and the difference in the diameter of the particles is not great, it is appropriate to define the minimum of r as a multiple of dp. Furthermore, the increasing step size of r is also defined as a multiple of dp.

On the other hand, to judge whether the phase morphology has self-similarity, the scale function $S_M(r)$ is introduced.

$$S_M(r) = M(r) \cdot r^{-D} \tag{C4}$$

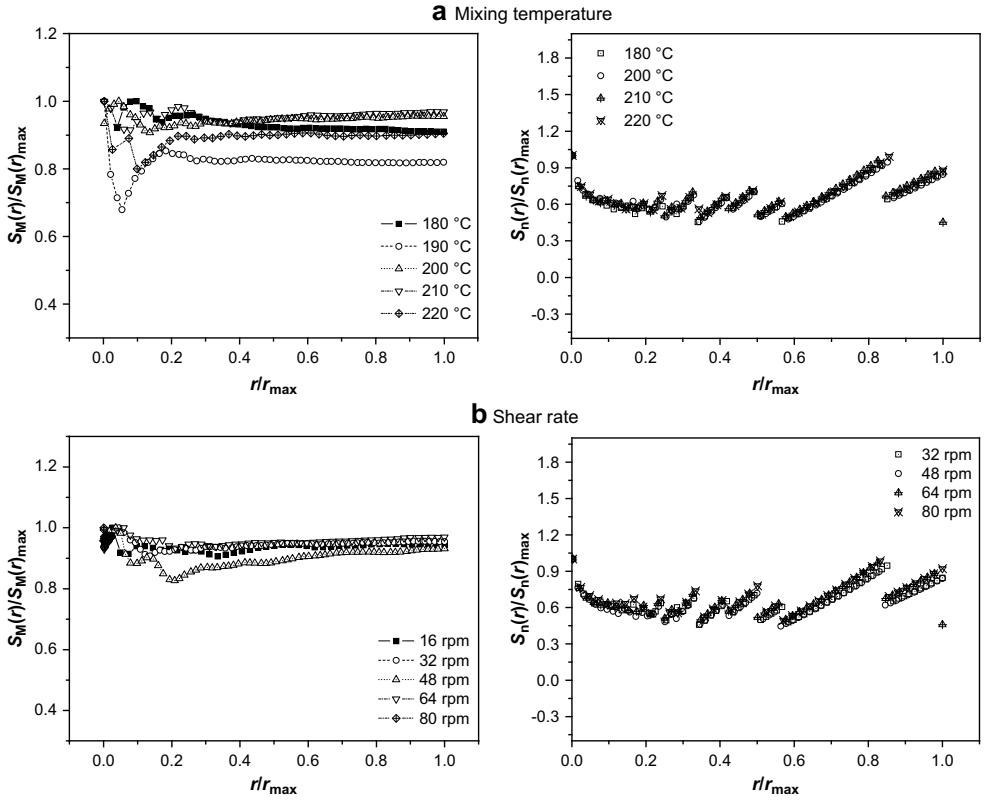

Fig. 16. Scale function $S_M(r)/S_M(r)_{max}$ and $S_N(r)/S_N(r)_{max}$ in PP80/mEP20 blends with mixing temperature and shear rate.

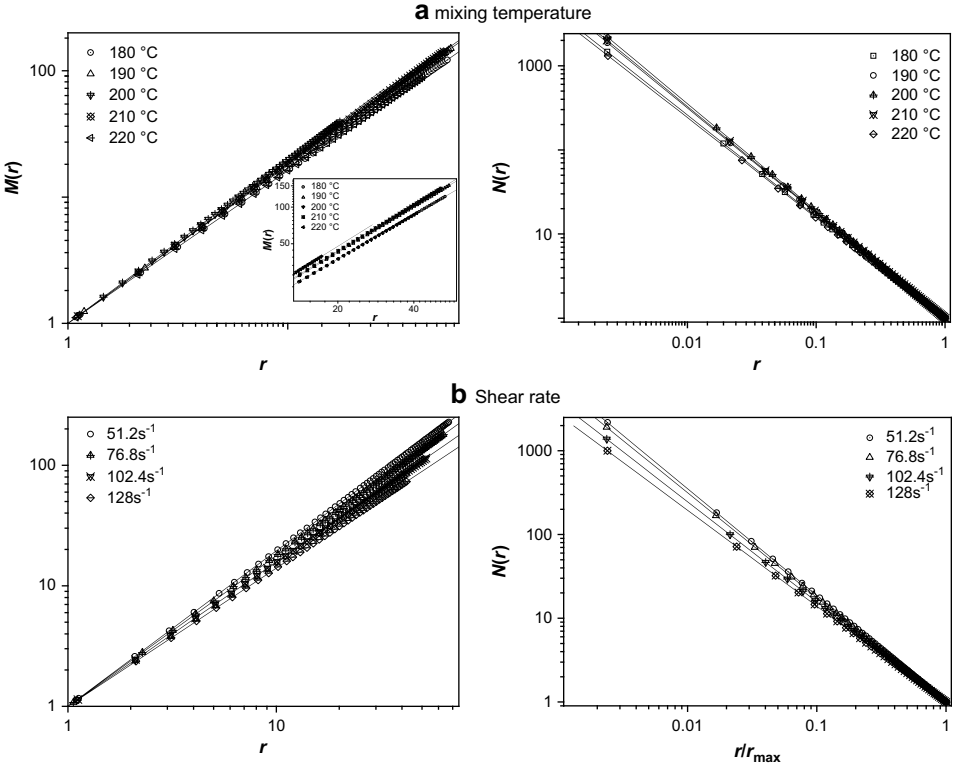

Fig. 17. A plot of log $M(r)$ and log $N(r)$ against log r and the fractal dimensions D of the phase morphology in PP80/mEP20 blends with mixing temperature and shear rate.

As r increases, if $S_M(r)$ fluctuates within a small range, it means that the complexity of the phase morphology does not depend on the change of r, or the phase morphology has self-similarity. Then it is appropriate to study the fractal dimension.

References

[1] Morero D, Santambrogio A, Porri L, Ciamoelli F. Chimica e l'Industria (Milano) 1959;A1:758.
[2] Paul DR, Bucknall CB. Polymer blends. New York: A Wiley-Interscience Publication, John Wiley & Sons; 2000.
[3] Deanin RD, Crugnola AM. Toughness and brittleness of plastics, American in chemistry series 154. Washington, DC: American Chemical Society; 1979. p. 284.
[4] Manchado MAL, Torre L, Kenny JM. Journal of Applied Polymer Science 2001;81:1063–74.
[5] Datta S, Naskar K, Jelenic J. Journal of Applied Polymer Science 2005;98:1393–403.
[6] Arroyo M, Bell M. Journal of Applied Polymer Science 2002;83:2474–84.
[7] Prut E, Medintseva T, Dreval V. Macromolecular Symposia 2006;233:78–85.
[8] Ma GQ, Yuan XB, Sheng J. Acta Polymerica Sinica (Chinese) 2002;1:63–7.
[9] Wilhelm HM, Felisberti MI. Polymer Bulletin 2004;51:419–27.
[10] Ichazo M, Hernandez M, Gonzalez J. Polymer Bulletin 2004;51:419–27.
[11] Ao NJ, Wang Q. Plastic Rubber Composites 2002;31:6–11.
[12] Sengupta P, Noordermeer JWM. Journal of Elastomers and Plastics 2004;36:307–31.
[13] Sheng J, Qi LY, Yuan XB. Journal of Applied Polymer Science 1997;64:2265–72.
[14] Ma GQ, Yuan XB, Sheng J. Journal of Tianjin University 2001;6:761–5.
[15] Yuan XB, Sheng J, Li XZ, Li JS, Cai ZJ. Acta Polymerica Sinica (Chinese) 2001;2:219–23.
[16] Ma GQ, Yuan XB, Sheng J, Bian DC. Journal of Applied Polymer Science 2002;83:2088–94.
[17] Ma GQ, Zhao YH, Yan LT, Li YY, Sheng J. Journal of Applied Polymer Science 2006;100:4900–9.
[18] Guo MY, Zhou XD, Dai G. Polymer Composites 2005;13:173–80.
[19] Wahit MU, Hassan A, Rahmat AR. Journal of Reinforced Plastics Composites 2006;25:933–55.
[20] Chiu HT, Hsiao YK. Journal of Polymer Research 2006;13:153–60.
[21] Wu H, Sun XL, Li Z. Journal of Macromolecular Science, Part B: Physics 2007;46:329–39.
[22] Akemi N, Toshio S, Wang W. Macromolecules 1996;29:5990–6001.
[23] Charoensirisomboon P, Inoue T. Polymer 2000;41:7033–42.
[24] Wang Y, Cai ZJ, Sheng J. Journal of Macromolecular Science, Part B: Physics 2004;43:1075–93.
[25] Li YY, Wang Y, Sheng J. Journal of Macromolecular Science, Part B: Physics 2005;44:665–76.
[26] Li YY, Wang Y, Li WQ, Sheng J. Journal of Applied Polymer Science 2007;103:365–70.
[27] Schreiber HP, Olguin A. Polymer Engineering and Science 1983;23:129–34.
[28] Plochcki AP, Dagli SS, Andrews RD. Polymer Engineering and Science 1990;30:741–52.
[29] Scott CE, Macosko CW. Polymer 1994;35:5422–33.
[30] Scott CE, Macosko CW. Polymer 1995;36:461–70.
[31] Elemans PHM, Bos HL, Janssen JMH. Chemical Engineering Science 1993;48:267–76.
[32] Yang YP, Li WQ, Xiao ZG, Li YY, Jiang X, Sheng J. Journal of Macromolecular Science, Part B: Physics 2006;45:1039–52.
[33] Yang YP, Xiao ZG, Jiang X, Sheng J. Journal of Macromolecular Science, Part B: Physics 2006;45:1083–96.
[34] Zhou JM, Sheng J, Zhang H. Acta Polymerica Sinica (Chinese) 1998;5:518–24.
[35] Zhang DH, Sheng J, Xie ZM, Li JS. Industrial and Engineering Chemistry Research 2002;19:141–6.
[36] Han CD, Jhon MS. Journal of Applied Polymer Science 1986;32:3809–40.
[37] Han CD, Kim JK. Macromolecules 1989;22:4292–302.
[38] Limpert E, Stahel WA, Abbt M. Biosciences 2001;51:341–52.
[39] Wu S. Polymer 1985;26:1855–63.
[40] Takayasu H. Fractal in the physical science. Manchester and New York: Manchester University Press; 1990. p. 11–4.
[41] Mandelbrot BB. Fractal geometry of nature. New York: Macmillan; 1983.
[42] Zhang JZ. Fractal. Beijing: Tsinghua University Press; 1995.
[43] Fang KT, Xu JL. Statistics distribution (Chinese). Beijing: Science Press; 1987. p. 136–58.
[44] Han YP, Sheng J. Chinese Journal of Light Scattering 2001;12:203–10.